AIAA AVIATION Forum
August 2-6, 2021, VIRTUAL EVENT
AIAA AVIATION 2021 FORUM

10.2514/6.2021-2762

Performance of Various Turbulence Models for Simulating Sub-critical High-Reynolds Number Flows over a Smooth Cylinder

Michael D. Mays* and Sylvain Laizet
Department of Aeronautics, Imperial College, London, UK

Sylvain Lardeau
Siemens Industry Software GmbH, Nürnberg, Germany

Simulating the flow over a smooth cylinder with low-level inlet turbulence for a Reynolds number equal to 140,000 remains a robust test case to evaluate the performance of turbulence closure models and numerical methods. This study considers a variety of closure levels, Reynolds-Averaged Navier-Stokes (RANS), Detached and Large Eddy Simulations (DES/LES) and hybrid RANS/LES, to determine their applicability to this case, with consideration given to their sensitivities to the spatial resolution and to the numerical schemes used. Neither the RANS nor DES closures selected in this study are able to capture the correct physical behaviour of the flow, largely due to weaknesses in the model formulations that prevent the formation of instabilities in the free shear layer. The LES Wall-Adapting Local Eddy-viscosity (WALE) model performs well with a sufficiently well refined mesh but it remains a computationally demanding method. A novel Scale Resolving Hybrid (SRH) model, formally derived from temporal filtering of the Navier-Stokes equations, shows an excellent agreement with experiment for the quantities of interest. The SRH model performs far better on a coarse mesh by comparison to other RANS and hybrid RANS/LES models and can produce results similar to the LES WALE model. The main conclusion of this work is that the robust behaviour of the SRH model, coupled with its potentially substantial reduction in computational demand, makes it an excellent candidate to study highly-separated external flows at high Reynolds numbers.

I. Nomenclature

C_p	=	time-averaged pressure coefficient
C_D	=	time-averaged drag coefficient
$\overline{C_D'^2}^{1/2}$	=	drag coefficient standard deviation
C_L	=	time-averaged lift coefficient
$\overline{C_L'^2}^{1/2}$	=	lift coefficient standard deviation
D	=	cylinder diameter
L_r, L_z	=	domain size in the radial and spanwise directions
L_{rc}	=	length of re-circulation bubble
N_r, N_θ, N_z	=	number of cells in the polar directions
N_{total}	=	total number of cells in mesh
Q	=	Q-criterion value
r, θ, z	=	polar coordinate system
r_{str}	=	grid stretching ratio in radial direction
U_∞	=	inlet/free-stream velocity
$\overline{U}$	=	time-averaged streamwise velocity
X, Y, Z	=	cartesian coordinate system
Δr^+, $\Delta\theta^+$, Δz^+	=	wall-adjacent cell sizes in time-averaged polar wall-units
Δr_1	=	width of first cell in radial direction

*PhD Student, Department of Aeronautics, mdm114@imperial.ac.uk

Δt	=	time step
ν_t, ν_{sgs}	=	turbulent viscosity, sub-grid scale viscosity
σ	=	upwinding blending factor
ϕ	=	DDES correction factor
ψ	=	SRH correction factor

II. Introduction

THE canonical case of the turbulent flow around a smooth cylinder at a Reynolds number (based on the free-stream velocity U_∞ and the cylinder diameter D) equal to 140,000 continues to present an excellent test case for numerical modelling research. The ability to accurately simulate this case is significant not only for its application to the ubiquitous real-word specific case of circular structures in cross-flow, but also as a representative case of highly-separated flow where the separation point is not geometry enforced. Critically, despite the symmetric configuration of the geometry and the simplicity of the case conditions, the internal physics of the case creates a high-sensitivity to the numerical methods chosen in simulating the case. This case is in the upper limit of the sub-critical flow regime where turbulent transition occurs in the free shear-layers, with the flow dynamics dominated by the spatial development of the Kelvin–Helmholtz rollers and turbulence onset.

The importance of this case to industrial applications has motivated an extensive number of numerical [1–6] studies to investigate the flow physics and to assess the performance of turbulence models in simulating such cases. The ability of turbulence models to correctly simulate turbulent flows for which the transition occurs in the free shear-layer is based on four physical phenomena: (1) the inception of the Kelvin–Helmholtz instability in the free shear-layer; (2) the spatial development of the Kelvin–Helmholtz vortices; (3) the breakdown to turbulence; and (4) the turbulent free shear-layer roll-up and vortex-shedding. The location of all these phenomena is Reynolds number dependent. When the Reynolds number is increased, the onset of instabilities in the free shear layer moves upstream towards the cylinder, leading to a more rapid spatial development of the Kelvin–Helmholtz vortices. As a result, simulation results are more likely to be sensitive to the near-wall behaviour of turbulence closure models.

One of the earliest numerical studies for the flow around a smooth cylinder at a Reynolds number equal to 140,000 is from [1]. The author aimed to investigate the influence of sub-grid scale modelling (SGS) in a Large Eddy Simulation (LES) context and mesh resolution on the quality of the predicted results. The simulations were performed on various meshes with the well-known Smagorinsky [7] and the dynamic sub-grid scale model [8]. Overall, LES results agreed fairly well with the experimental reference data, especially in the near wake. Discrepancies were reported in the far wake with a strong dependence on the mesh resolution. A strategy which blends a variational multi-scale large eddy simulation (VMS-LES) model and a RANS model in a hybrid approach was investigated in [2]. In particular, the sensitivities of the approach with respect to the mesh resolution, the SGS model and the definition of the blending parameter were studied. It was found that such hybrid approaches, where the model works in pure Reynolds-Averaged Navier-Stokes (RANS) mode in the boundary layer and in the shear layers, and in LES mode in the wake, can be beneficial to reduce the computational effort required to simulate such flows.

Further investigation of purely LES methods applied to the flow around a smooth cylinder around the drag crisis (a sudden drag reduction as the Reynolds number is increased, with a dramatic change in flow patterns) was conducted in [3]. The authors used the Wall-Adapting Local-Eddy viscosity (WALE) model LES model [9] on fine meshes to capture the drag crisis. Good agreement with experiments was reported, with three different flow configurations observed around the drag crisis: one-bubble asymmetric mode, two-bubble asymmetric mode and two-bubble symmetric mode. The study by [10] questioned the widespread scepticism towards the application of Unsteady-RANS (URANS) based methods for massively separated generic flows over a bluff body. The authors provided a theoretical basis for the applicability of the URANS approach for such flows and concluded that, while conventional linear-eddy viscosity RANS models cannot accurately simulate this case, it appears that higher-moment Reynolds Stress Model (RSM) RANS closures can perform well for the flow around a smooth cylinder around the drag crisis. More recently, [5, 6] investigated seven RANS and Scale-Resolving Simulation (SRS) methods: RANS with the Shear-Stress Transport (SST) [11] with and without the Local-Correlation Transition Model (LCTM) [12], RANS Explicit Algebraic Reynolds-Stress Model (EARSM) [13], Delayed Detached-Eddy Simulation (DDES) and Improved DDES (IDDES) [14], eXtra Large-Eddy Simulation (XLES) hybrid models [15], and Partially-Averaged Navier–Stokes equations (PANS) method [16].

The motivation of this work is to assess the performance of various turbulence models ranging from LES to RANS to capture the main features of the flow around a smooth cylinder for a Reynolds number equal to 140,000, such as the separation behaviour, onset and development of the instability mechanism underlying the break-down of the

shear-layer and production of vortex shedding. In particular, the behaviour of a new hybrid model [17] derived from a temporal filtering formalism used to control the energy partition between resolved and modelled turbulent scales will be discussed in detail and compared with more well-known models. Specifically, the following models will be examined: the $k-\omega$ Shear Stress Transport (SST) model [18] in its URANS, DDES and novel SRH modes, with or without the Gamma-ReTheta (γRe_θ) transition model[19]; a Lag Elliptic Blending $k-\epsilon$ model [20] in both URANS and novel SRH modes; an Elliptically Blended Reynolds Stress Transport model [21]; and finally the major LES models: Smagorinsky [7], Dynamic Smagorinsky [8] and WALE models [9]. Given that the accurate prediction of separation and transition play a key role in assessing the forces experienced by a body, the simulations will be primarily assessed using the predicted time-averaged drag coefficient and related time-averaged pressure coefficient profiles around the cylinder. A broader consideration of results will be used to determine the cause of success or failure and the idiosyncrasies of each turbulence models. The major focus of the study is to consider which turbulence model presents the strongest case for general use in an industrial context and, in that regard, particular attention will be paid to the hybrid RANS/LES methods which potentially offer a significant reduction in computational cost while retaining accuracy.

This manuscript is structured as follows. Section III lays out an detailed description of the case to be simulated with the relevant numerical methods and the different mesh parameters. A discussion of the salient features of each of the aforementioned closure models is also included. Section IV presents the key results from each of the cases and a discussion of the significance of those results relevant to each of the levels of turbulent models. Finally, Section V concludes by giving an overview of the main results and points of discussion in relation to the focus of the study.

III. Flow Physics and Numerical Parameters

A. Flow details

The case examined here is the canonical case of low-level inlet turbulence flow over a smooth 'infinite-length' cylinder at a Reynolds number equal to 140,000. This flow is in the sub-critical regime meaning that the transition to turbulence takes place in the free shear layers, post-separation of the boundary layers. However, at this Reynolds number the development of the instabilities that lead to transition occurs very near to the cylinder wall. For this reason, in conjunction with the difficultly in precisely predicting the separation point and the free shear layer breakdown, the case, despite its simple geometry, presents a significant challenge for turbulence closure models and numerical schemes. This is particularly true for hybrid methods that change behaviour in the vicinity of the wall. A detailed discussion of the physics involved in this case and the other regimes of vortex shedding can be found in [22].

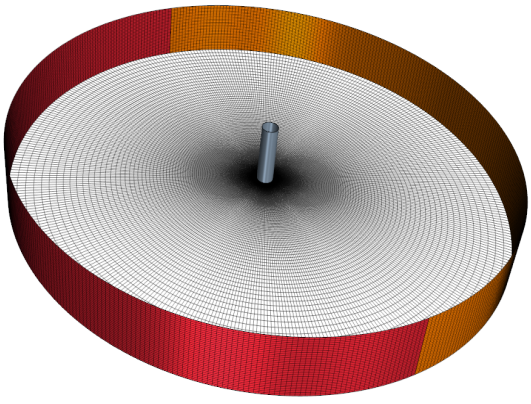

Fig. 1 Computational domain ($L_r = 30D$) indicating inlet (red) and outlet (orange).

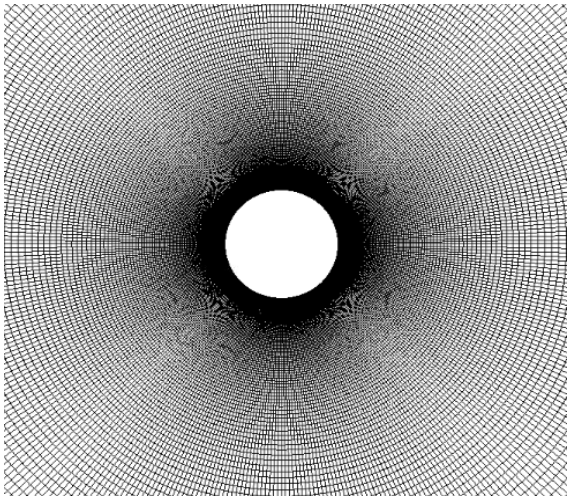

Fig. 2 Central zone of O-mesh ($r-\theta$ plane) used for simulations.

B. Domain and mesh parameters

The simulations are conducted on an O-type mesh based on the mesh used by [1] in his earlier studies of LES applied to flow around a cylinder. The domain, seen in Fig. 1 with the inlet and outlet in red and orange, respectively, is $30D$ in diameter with the cylinder of diameter D at the centre. The spanwise length L_z varies between the meshes, with the values shown in Table 1. An example of the inner zone of one of the meshes can be seen in Fig. 2. This type of mesh only requires the number of cells in each of the three directions and the distance of the first cell from the wall, which gives the stretching in the radial direction, to completely define it. The radial stretching allows the near wall cells to resolve the boundary layer but leaves the cells at the boundaries very large. Stretching can have a negative effect on the accuracy of the results and it is important, therefore, to use a sufficient number of cells in the radial direction to ensure that the stretching factor remains small, e.g. $r_{str} < 1.05$. The mesh parameters used throughout this study are shown in Table 1. The resolution of mesh A is based on [10], mesh B is a replica of the coarse mesh of [1] and mesh C is a more highly refined version of these meshes. A small time-step, in line with the previously mentioned studies, is chosen throughout to prevent issues with inadvertent filtering of the field. This choice of time step yields a time-averaged convective Courant number between 1 and 2 for all the cases.

Table 1 Mesh parameters and time steps used for simulations, with wall-unit measurements based on the time-averaged wall $\Delta\theta^+$ value from the simulation with the WALES LES model on mesh C.

Mesh	N_r	N_θ	N_z	L_z/D	$\Delta r_1/D$	$\Delta r^+ \times \Delta\theta^+ \times \Delta z^+$	$\Delta t U_\infty/D$	N_{total}
A	238	400	32	3	2×10^{-4}	$1.3 \times 60.0 \times 721.1$	2×10^{-3}	2995200
B	165	165	64	2	4×10^{-4}	$1.3 \times 146.5 \times 240.4$	2×10^{-3}	1742400
C	220	600	128	2	2×10^{-4}	$1.3 \times 40.3 \times 120.2$	2×10^{-3}	16890000

C. Numerical methods

The simulations are performed with the commercial software Simcenter STAR-CCM+, a second-order accurate finite-volume code [23]. The time integration is achieved with a backward second-order implicit time integration scheme, with the number of inner iterations chosen to ensure residuals for the momentum, continuity and turbulence quantity equations fall below 1×10^{-5}. The diffusion term is discretised using the second-order central difference scheme and the discretisation of the convective term varies as discussed below.

1. Turbulence models

The choice of closure model for the proposed simulations, both in level of closure, i.e. RANS, hybrid RANS/LES or LES, and specific tuning and variations within each level is the main focus of this study. The fully RANS models considered here are two linear-eddy viscosity models, the $k-\omega$ SST model devised by Menter [18], with minor modifications, and a Lag Elliptic-Blended (EB) $k-\epsilon$ (LEBKE) model [20] which solves two additional transport equations to better account for transition and non-linear behaviours, and an Elliptic-Blended (EB) Reynolds Stress Model (RSM) [24], the closest model in design to that used in [10]. These three models solve an increasing number of transport equations reflecting a theoretically improved ability to accurately capture complex flow features by accounting for non-linear and non-isotropic behaviours.

For the hybrid models this study considered the Delayed Detached Eddy Simulation (DDES) model [25, 26] based on the $k-\omega$ SST URANS model and a Scale Resolving Hybrid (SRH) model [17] using both the $k-\omega$ SST and Lag EB $k-\epsilon$ models as bases. The $k-\omega$ SST DDES model, like the majority of hybrid methods, involves the alteration of one of the transport equations of the RANS model creating a sensitivity to the grid spacing in an LES fashion. In this case the specific dissipation term ω in the destruction term of the turbulent kinetic energy k transport equation is substituted with a modified specific dissipation $\tilde{\omega} = \omega\phi$, where ϕ is the DDES Correction Factor. Of particular note is the use of a shielding function designed to prevent inappropriate transition to LES behaviour by the model in areas of meshes that do not have sufficient resolution to sustain it. Consideration was also made of this model used in conjunction with the two-equation γRe_θ transition model [19]. This model is designed to mitigate issues with turbulence closure models that erroneously predict a premature transition to turbulence.

The SRH model proposed by [17] is highly similar in form to the DDES model. As with DDES, the SRH model introduces an altered dissipation ϵ or specific dissipation ω, depending on the chosen basis RANS model, into the

destruction term of the sub-filter turbulent kinetic energy transport equation using a variable ψ, here termed the SRH correction factor, the major difference between the two models being the ways in which ϕ and ψ are determined. One major advantage of the SRH model is its derivation from a temporal filtering formalism which allows an analytical determination of most of the key model parameters. Again, like the DDES, but of a different form, the SRH model uses a shielding function to enforce RANS behaviour in the near-wall region. The consideration of this shielding in the hybrid methods will be of key importance for the results and for general understanding of the hybrid methods.

Finally, the major LES models are also considered: Smagorinksy[7], Dynamic Smagorinsky [8, 27] and WALE models [9]. The Smagorinsky model was used with van Driest damping of the same form used by [1] to achieve accurate near wall behaviour. The exact formulations and numerical treatments of each of these models may be found in the Simcenter STAR-CCM+ documentation [23].

2. Convection discretisation schemes

The choice of the discretisation scheme, and relevant parameters, used with each model is an important factor for this case. The default convective scheme for LES in Simcenter STAR-CCM+ is a Bounded Central Difference (BCD) scheme, which uses a second-order Central Difference (CD) scheme blended with a second-order upwinding scheme provided a local boundedness criterion is satisfied. If a cell fails the boundedness criterion it reverts to a first-order upwinding scheme. An alternative, the MUSCL/third-order (MUSCL) scheme, also a bounded hybrid upwind/central difference scheme, is considered. This bounding provides a stable and robust behaviour but could potentially have negative effects on the results. The level of upwinding introduced in each of these schemes is controlled by the upwinding blending factor σ. In order to examine the effect of bounding an unbounded pure second-order central difference scheme is considered. The recommended scheme for hybrid RANS/LES methods is a Hybrid-BCD scheme which transitions from a second-order upwinding scheme in the RANS region to the aforementioned BCD scheme in the LES zone. For the RANS simulations the conventional second-order upwinding scheme is used.

D. Boundary/Initial conditions and time-averaging

For the boundary conditions, the inlet is a fixed velocity in the streamwise direction necessary to give the correct Reynolds number based on the cylinder diameter and fluid viscosity (here $D = U_\infty = 1$ and $\nu = 1/140000$), and no inlet turbulence as per the case definition. In simulations using URANS, very low-level inlet turbulence is used for the duration of the initialisation period, with statistic collection beginning after the effect is washed out and the turbulent field is fully developed. This is done to initialise the solving of the turbulence equations which might otherwise remain dormant, often leading to a failure to accurately predict the turbulent transition. For the LES cases the flow field is initialised throughout as equal to the inlet velocity. However, for the URANS and hybrid cases the field is initialised using results from a prior URANS simulation with a fully developed turbulent field. In the spanwise direction a periodic boundary condition is used to achieve the 'infinite-length'-like behaviour and to attempt to mitigate effects associated with aspect ratio (L_z/D) choice. Finally, for the outlet a prescribed pressure value is used across the boundary. While this could potentially introduce erroneous pressure reflections into the domain these were not observed throughout the simulations run here and appeared to have no significant negative impact. To achieve good convergence of the time-averaged statistics the simulation must be run over many vortex cycles, as discussed in [28]. For this study, the simulations are performed for an initialisation period after which the statistics were collected at each time step for at least 50 vortex shedding cycles and up to 75 for LES cases.

IV. Results

A selection of results is presented in this section in order to assess the performance of the turbulence models under scrutiny. We consider the suitability of different closure methods in being applied to this case and, further, the most ideal choices of numerical methods applicable to those. A summary of the cases run and the numerical results is shown in Table 2.

A. RANS methods

Based on previous studies where RANS methods were applied to this case, a series of simulations using variants of RANS models are conducted on mesh A with the parameters indicated in Table 1. It is clear from the C_D values in Table 2 and the substantial difference between the predicted and the experimental C_P distributions around the cylinder surface, seen in Fig. 3, that none of the RANS formulations are capable of matching the experimental reference data. It

is noteworthy, however, that as the number of additional transport equations solved increases the results do improve, with the EB-RSM proving to be most accurate approach for this type of simulations.

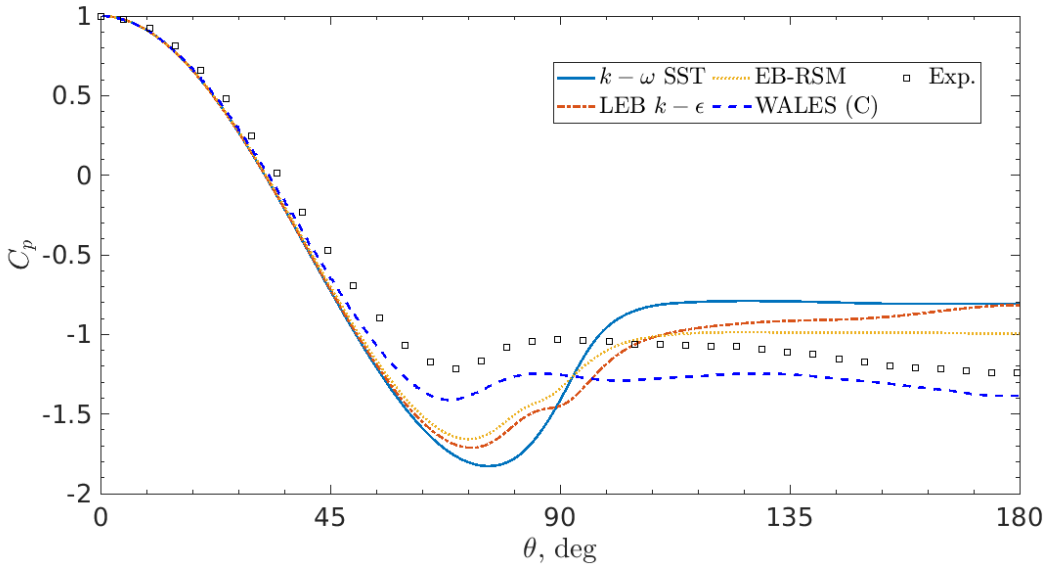

Fig. 3 Time-averaged pressure coefficient C_p distribution around cylinder for different RANS closure levels with WALES (C) and experimental reference data [29].

The failure of the $k-\omega$ SST URANS model is not unexpected and has been commented on in many studies, see for instance [6, 10]. This is largely attributable to two major failings: a premature transition to turbulence as noted in [30], and an inability to sufficiently resolve the instabilities in the shear layer. The premature transition to turbulence causes the simulation to produce results more in line with higher Reynolds number flow in the super-critical regime of vortex shedding in which the now turbulent boundary layers remain attached for longer, delaying separation and leading, consequently, to a reduction in the drag experienced by the cylinder. This is highlighted by considering the time-averaged boundary layer profiles seen in Fig. 4. The $k-\omega$ SST DDES result is essentially identical to the URANS results (not shown) for reasons discussed later on and we can see that, in contrast to the Lag EB $k-\epsilon$ and EB-RSM models, the $k-\omega$ SST model does not show flow reversal, indicative of flow separation, even past 95^o over the cylinder surface.

The Lag EB $k-\epsilon$ and EB-RSM models, on the other hand, do not share the same issue with premature transition which is demonstrated by the clear presence of flow reversal in the boundary layer profile by the 90^o position on the cylinder surface. These two models behave similarly with similar C_p distributions, as seen in Fig. 3, and show clear improvement over the $k-\omega$ SST model's distribution, most notably with the presence of an inflection point around the point of separation, similar to the reference WALES (C) data. Nonetheless, neither model is capable of adequately predicting mean or fluctuating force data and the re-circulation bubble is overly broad and long when compared with WALES LES results on the C mesh, as seen in Fig. 8 or when compared to experimental reference values for the re-circulation length in Table 2.

The failure in these cases, which is shared by the $k-\omega$ SST model, is due to the inability to adequately capture the onset and development of the free shear layer breakdown. This is most clearly visible in the instantaneous visualisations of the Q-criterion iso-surfaces shown in Fig. 13. The separated shear layers of the $k-\omega$ SST and EB-RSM models both clearly remain stable well past the cylinder when compared with the WALES (C) case where the breakdown is almost instantaneously post-separation. Close examination of the iso-surfaces shows that the $k-\omega$ SST and EB-RSM differ in that, while the $k-\omega$ SST model shear layer is always stable, the shear layer in the EB-RSM model shows an initial area of instability before re-stabilising. This suggests that the EB-RSM model, in its present formulation, is capable of capturing some unsteady flow features but not to the degree necessary to see full shear layer breakdown. Work in [6] yielded a condition on the required effective Reynolds number, which can be viewed effectively as the inverse of turbulent or sub-grid viscosity, in the vicinity of the free shear-layer necessary to observe the correct breakdown behaviour. This condition would indicate that the RANS models are over-predicting the turbulent viscosity owing to an

Table 2 Comparison of numerical results for each turbulence closure model with mesh indicated and reference experimental data taken from [29] and [31].

	Turb. Model	σ	Mesh	$\bar{C}_D$	$\overline{C_D'^2}^{1/2}$	$\bar{C}_L$	$\overline{C_L'^2}^{1/2}$	L_{rc}
Laminar	–	–	B	0.517	0.044	0.025	0.208	0.47
RANS-based	$k-\omega$ SST URANS	–	A	0.770	0.041	0.008	0.198	0.96
	Lag EB $k-\epsilon$ URANS	–	A	0.819	0.042	0.009	0.214	0.84
	EB RSM	–	A	0.921	0.045	0.015	0.321	0.86
Hybrid RANS/LES	$k-\omega$ SST DDES	0.00	A	0.700	0.033	-0.005	0.108	1.24
	$k-\omega$ SST DDES + γRe_θ	0.00	A	0.695	0.035	0.001	0.171	1.04
	$k-\omega$ SST SRH	0.00	A	0.813	0.058	-0.004	0.121	0.91
	$k-\omega$ SST SRH + γRe_θ	0.00	A	1.078	0.067	0.005	0.231	1.17
	Lag EB $k-\epsilon$ SRH	0.00	A	1.225	0.096	0.014	0.295	0.61
LES	Smag.	0.05	B	1.058	0.120	-0.002	0.389	1.05
	Dyn. Smag.	0.05	B	0.542	0.051	0.001	0.232	0.53
	WALES	0.05	B	0.526	0.045	0.002	0.225	0.49
	WALES	0.05	C	1.451	0.127	0.043	0.927	0.45
	WALES - MUSCL	0.05	C	1.472	0.116	-0.039	0.893	0.39
	WALES - CD	0.05	C	0.521	0.032	-0.019	0.177	0.79
	WALES*	0.00	C	1.287	0.153	0.033	0.491	0.68
Experiment		–	–	1.237	~ 0.18	0.000	~ 0.4	0.44

*Used as WALES (C) reference data

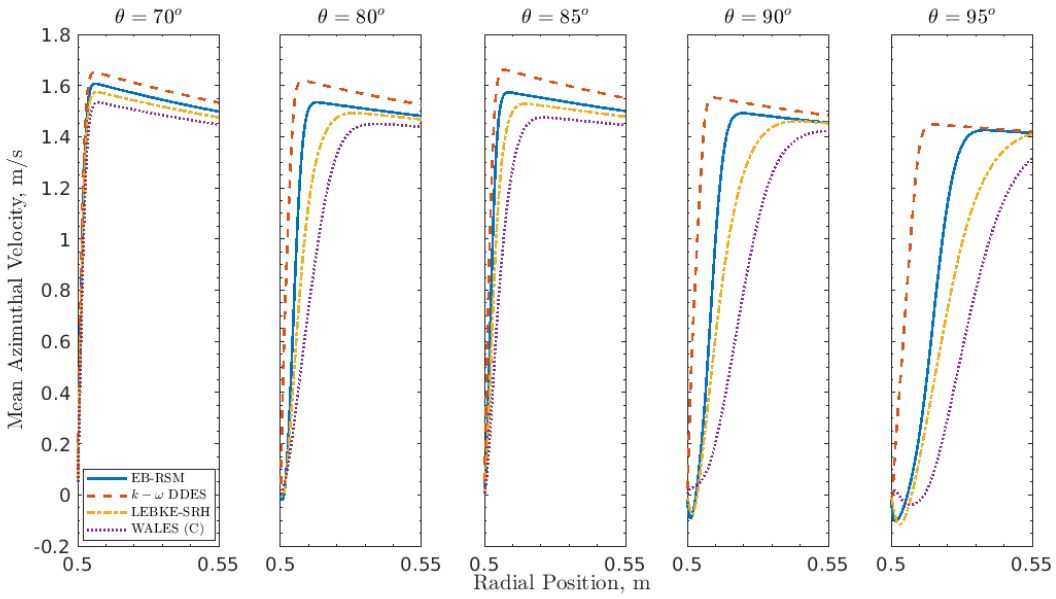

Fig. 4 Time-averaged boundary layer profiles at various angular positions over the top of the cylinder for representative closure models.

under-resolution of the turbulent field in the very-near-wall area. The results of this study are in line with that condition when the maximal values of time-averaged turbulent viscosity in Table 3 are considered. The high levels of turbulent viscosity in the shear layers prevents instability from forming in the $k-\omega$ SST case and causes the shear-layer to re-stabilise for the EB-RSM. However, this does provide an understanding of why the EB-RSM model performs the best of the URANS models.

The overall failure of the RSM model here is at odds with the results in [10], where the RSM gave good agreement with the experimental value of C_D, with the ability to capture low-frequency fluctuations in the velocity field, indicative of Kelvin-Helmholtz rollers present in the shear layer breakdown. There are possible reasons that can account for this disagreement, most notably the use of a total-variation diminishing (TVD) scheme that was not available for this study, as well as minor differences in the way the terms of the RSM are formulated. Nonetheless, it would appear that the effectiveness of higher-moment URANS methods remains sensitive to numerical choices rendering its general applicability suspect. Further investigations will be carried out to try to better understand the behaviour of the RSM model and its sensitivity to the numerical methods.

B. LES methods

LES closures remain the most popular methods found in literature for treating this case, though they remain computationally expensive despite the geometric simplicity of the configuration. Presented here are the results for the LES models used in this numerical study. The information garnered can inform not only further LES usage but also the behaviour of the LES-zones of the hybrid models. In previous studies, both the Smagorinksy model and the WALE model have been used to varying degrees of success. Here both models were applied to mesh B, a mesh identical to that employed by [1] in which the Smagorinksy model was found to perform very well.

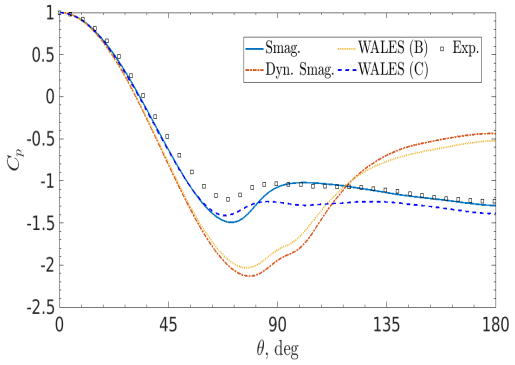

Fig. 5 Time-averaged pressure coefficient C_P distribution around cylinder for LES closures.

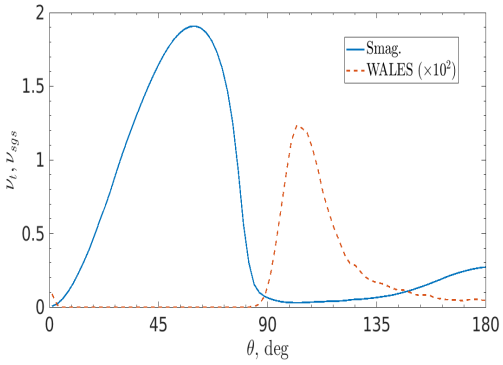

Fig. 6 Time-averaged turbulent or sub-grid viscosity ν_t, ν_{sgs} at $r = 0.501$m.

It would appear from the C_P distributions in Fig. 5 and the corresponding C_D values from Table 2 that the Smagorinsky model gives better agreement with the experimental values. This conclusion is, however, undermined by some other behaviours, notably the sub-grid viscosity ν_{sgs} profile at $r = 0.501$ m, as seen in Fig. 6. Given that the transition to turbulence should take place post-separation a significant rise in the sub-grid viscosity prior to the separation point would not be expected. However, a rise in sub-grid viscosity prior to separation is displayed by the Smagorinksy model but not by the WALE model. A case using the WALE LES model at a much increased resolution on mesh C is also shown in Fig. 5. When compared to the low-resolution WALES LES simulation on mesh B, an improved agreement with the experimental C_P distribution was found and the very-near-wall behaviour of the sub-grid viscosity remained the same. This would suggest that while the Smagorinsky model achieved a good result, it cannot be fully trusted to always do so and that the resolution used in [1] is insufficient for converged LES studies. This is supported by the author in [1] who observed further divergence from reference data with increased spatial resolution. The WALE LES model, on the other hand, when used at spatial resolutions more in line with recommended values for resolving turbulent boundary layers, can achieve a good agreement with reference data without erroneous physical behaviour. Looking at instantaneous visualisations of the Q-criterion iso-surfaces in Fig. 13, it can be seen that the increase in resolution for the WALE LES cases leads to a significant increase in the range of resolved turbulent scales, particularly in the shear layer and the re-circulation bubble. As discussed, capturing the physics in these regions is crucial for accurately

predicting the C_p distribution and forces on the cylinder. This is also supported by the shift in the qualitative behaviour of the time-average sub-grid viscosity field when compared to the URANS methods in Fig. 9. The sub-grid viscosity is dispersed throughout the wake rather than concentrated in the re-circulation bubble, supporting the notion that the structures in the bubble are far more resolved using the WALE LES model. The maximum value of sub-grid viscosity seen in Table 3 is also at least one order of magnitude smaller than any of the URANS methods. These results support the use of the WALE LES model for further analysis. Its poor result on the coarse mesh B compared to the Smagorinsky model, while undesirable, is based on accurate physical behaviour and requires the resolution expected in LES methods.

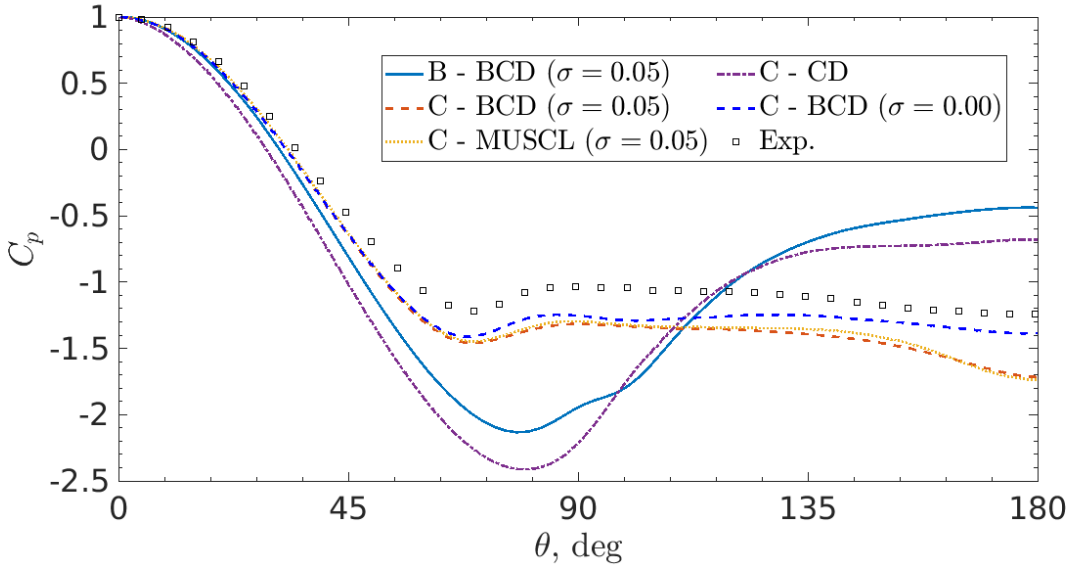

Fig. 7 Time-averaged pressure coefficient C_P distribution for WALES using different convective discretisation schemes with experimental reference data [29].

Having settled on the WALE LES model as the ideal choice for further study important consideration had to be given to the influence of the choices of numerical scheme. The main choices to be made are between unbounded or bounded schemes and, if bounded, the level of upwinding introduced into the scheme. In terms of the first choice, the resulting C_p profiles in Fig. 7 clearly show against choosing an unbounded pure central-difference scheme. It is likely that the presence of large cells closer to the boundaries dominated by convection are unstable under pure central-difference. This introduces erroneous sub-grid viscosity upstream of the cylinder that triggers a premature transition to turbulence causing the case to behave more like the super-critical regime, i.e. transition prior to separation of the boundary layer. It would appear then that some form of bounding is desirable on meshes that do not have highly refined cells throughout the totality of the mesh which is desirable for reducing computational cost.

Given then that the bounded central difference appears more desirable we consider further the bounded scheme and, in particular, the introduction of upwinding in the bounded cells. This is done to improve robustness of simulations and a default value of the upwinding factor $\sigma = 0.15$ is recommended by Simcenter STAR-CCM+. In Fig. 7 cases with no introduced upwinding and slight upwinding are compared. It is clear that for this case the upwinding is not necessary for stability but its introduction degrades the results, particularly in terms of the back pressure of the cylinder. This area of re-circulation is turbulent and is sensitive to the dissipative effects introduced by upwinding. We can conclude that the bounding of the scheme is sufficient to prevent any of the instability displayed by the unbounded scheme but that bounded upwinding can negatively affect the desired LES behaviour. Consideration of the bounded MUSCL scheme that is third-order central-difference when bounded was also made but showed no improvement over the standard second-order bounded scheme. There may be some advantage to using the third-order scheme for the resolution of the wake but as the mesh was relatively coarse in the wake of the cylinder, its effect was not seen.

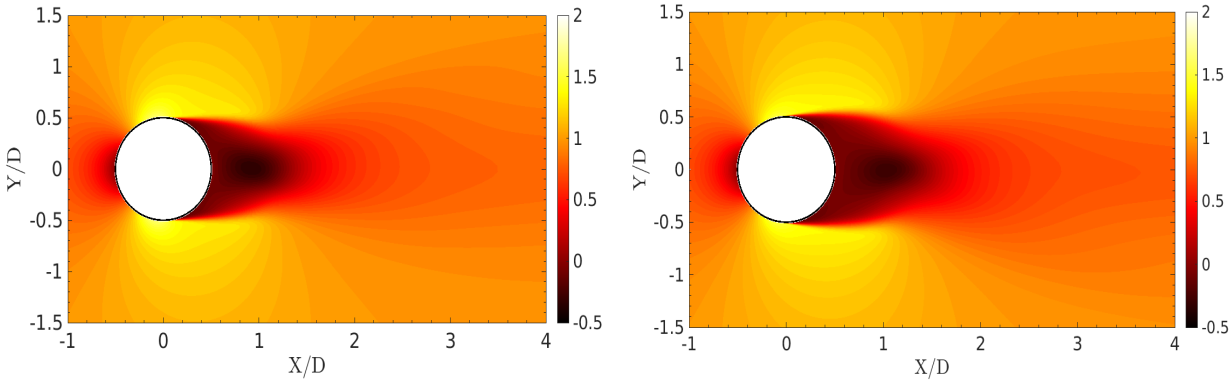

(a) $k-\omega$ **SST (A)** **(b) EB-RSM (A)**

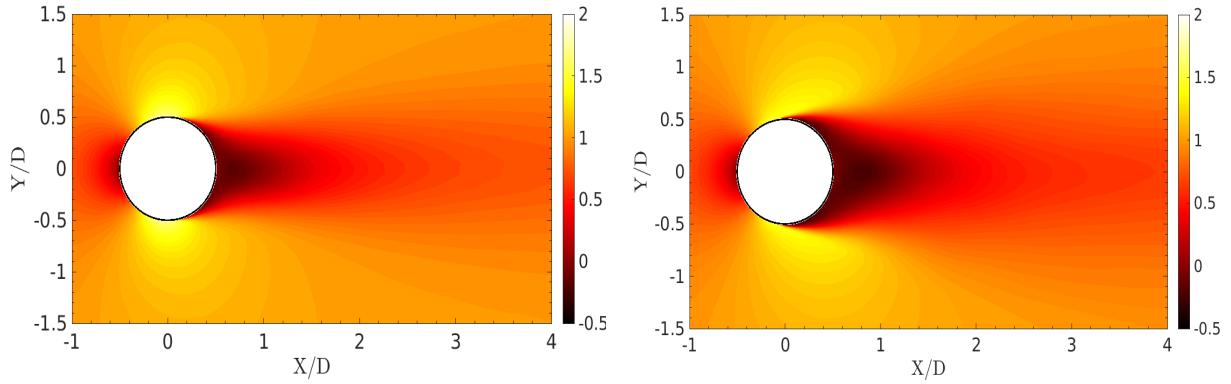

(c) WALES (B) **(d) WALES (C)**

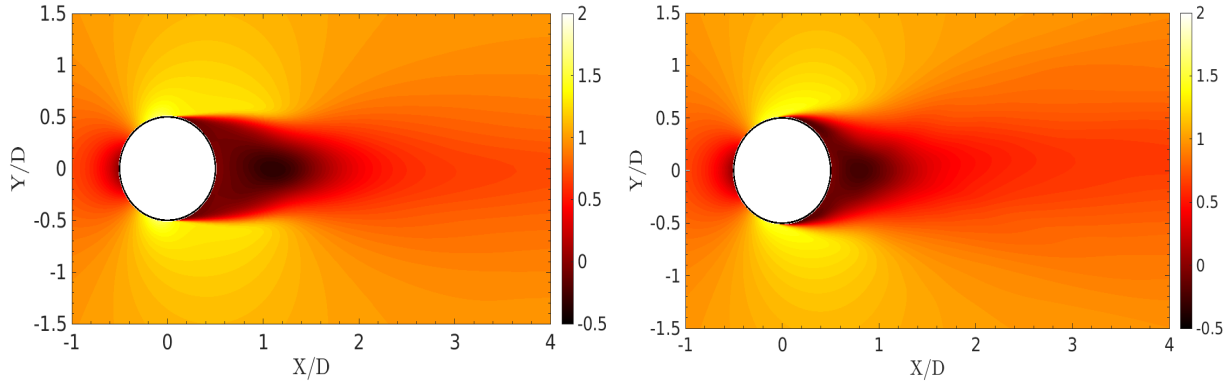

(e) $k-\omega$ **SST DDES (A)** **(f) LEBKE-SRH (A)**

Fig. 8 Time-averaged streamwise velocity $\bar{U}$ fields for major models with mesh indicated in brackets.

Table 3 Maximum values of time-averaged turbulent or sub-grid viscosity ν_t, ν_{sgs}

	a) $k-\omega$ URANS	b) EB-RSM	c) WALES B	d) WALES C	e) $k-\omega$ DDES	f) LEBKE-SRH
ν_t,ν_{sgs}	1005.0	754.0	65.8	33.6	258.0	13.1

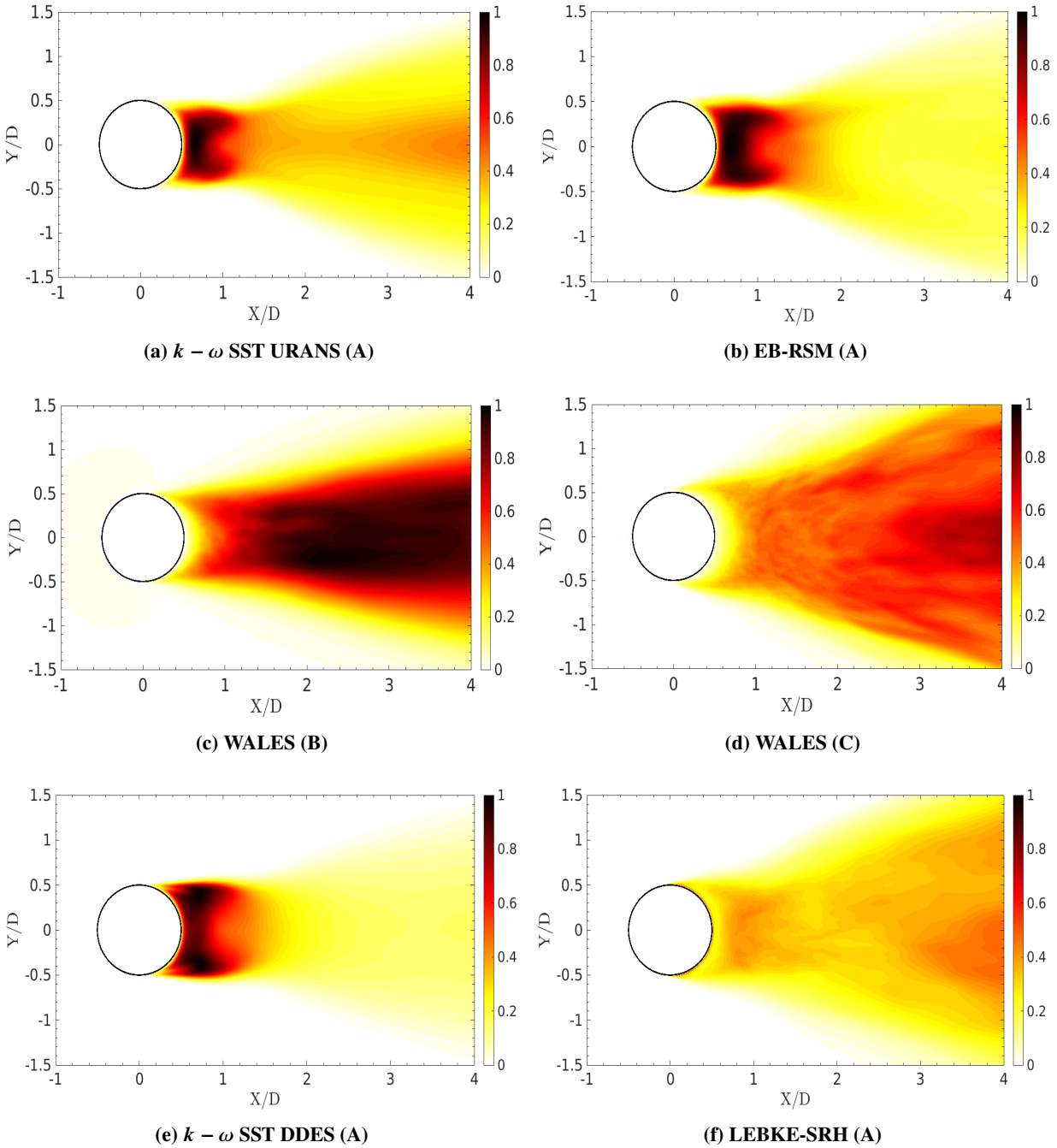

(a) $k-\omega$ SST URANS (A) **(b) EB-RSM (A)**

(c) WALES (B) **(d) WALES (C)**

(e) $k-\omega$ SST DDES (A) **(f) LEBKE-SRH (A)**

Fig. 9 Time-averaged turbulent or sub-grid viscosity ν_t, ν_{sgs} fields normalised by maximum values seen in Table 3 for major models with mesh indicated in brackets.

C. Hybrid RANS/LES methods

Hybrid RANS/LES closure models are the most novel methods for treating this case and they have the potential to provide near LES performance on a RANS mesh. Here we consider the results from the DDES model based on the $k-\omega$ SST model and use it as a basis for comparison with the novel SRH model. Both models are used with the hybrid convective scheme discussed in Section IIIc using $\sigma = 0$ for the BCD scheme used in the LES-like zones in line with the conclusions of the previous section.

1. DDES results

The results for the DDES are again summarised in Table 2 and the C_P profiles are shown in Fig. 10. As with previous studies found in literature [6], the DDES model does not present good agreement with experimental data for this case. It seems that the model being based on the simple linear eddy-viscosity $k-\omega$ SS model is a significant flaw for the base $k-\omega$ SST DDES as it preserves the premature transition to turbulence predicted by RANS models. As such, it yields an almost identical C_p profile to that of the $k-\omega$ SST URANS profile seen in Fig. 3. This similarity is further highlighted by similar time-averaged streamwise velocity fields, as seen in Fig. 8, and time-averaged turbulent viscosity fields, as seen in Fig. 9. A case was also performed using the γRe_θ transition model in an attempt to try to mitigate this limitation of the $k-\omega$ SST model. While this offers some improvement in the qualitative behaviour of the results, such as introducing an inflection in the C_p profile, there is essentially no change in the value of the predicted time-mean drag coefficient when compared to the case without the transition model.

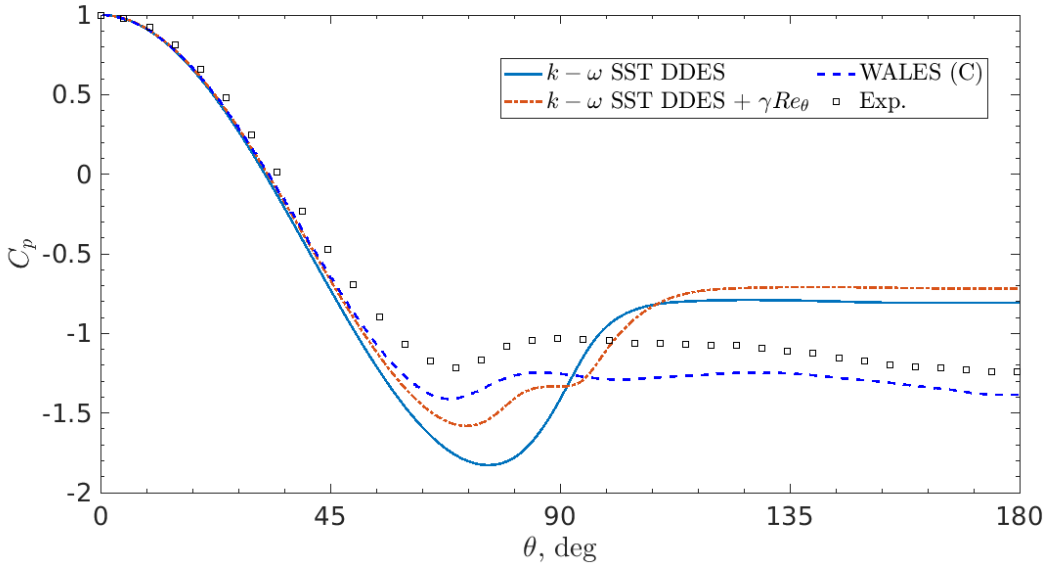

Fig. 10 Time-averaged pressure coefficient C_P distribution around cylinder for DDES closure models with WALES (C) and experimental reference data [29].

We see then that, at least in the near wall region, the $k-\omega$ SST in its DDES formulation remains essentially similar to the URANS formulation and does not appear to switch to an LES-like behaviour in the vicinity of the cylinder. The failure to switch modes is demonstrated in Fig. 14a where the DDES correction factor ϕ remains at 1, indicating pure RANS behaviour, in a wide band around the cylinder, increasing only further into the wake. This means that the DDES, as in the URANS, fails to adequately resolve unsteady fluctuations necessary to capturing the correct breakdown mechanism of the shear layer. This is demonstrated by the Q-criterion iso-surfaces in Fig. 13 where, like the $k-\omega$ SST URANS and EB-RSM, the shear layer remains coherent far past the cylinder, though the $k-\omega$ SST DDES formulation does show a greater range of resolved scales in the re-circulation bubble than in the pure URANS formulation. It is further highlighted by Fig. 11 showing an instantaneous realisation of the spanwise vorticity where the shear layer shows no sign of Kelvin-Helmholtz rollers or breakdown. This is confirmed by continued high levels of sub-grid viscosity from Table 3 compared with the WALE LES or SRH models and where the distribution of sub-grid viscosity shown in Fig. 6 is more qualitatively similar to the URANS methods than the other scale resolving methods.

As discussed in the introduction, the DDES model incorporates a shielding function to prevent the model switching to LES-mode near to the wall. The current formulation of the shielding function, however, appears to be over-shielding, actively preventing a transition to LES-like behaviour all around the cylinder. Potentially, the alteration of the shielding function to allow for a significantly earlier transition to LES mode, especially in the shear layer, coupled with the use of a transition model to mitigate the issues of premature transition in the boundary layers could allow reasonable results to be obtained from a DDES model. Doubts must be raised however by previous studies which have indicated a very slow development of LES content in DDES, independent of shielding considerations unless the DDES model is altered further [32]. This may limit the ability of the DDES formulation to accurately locate the onset of the instability and capture its spatial development.

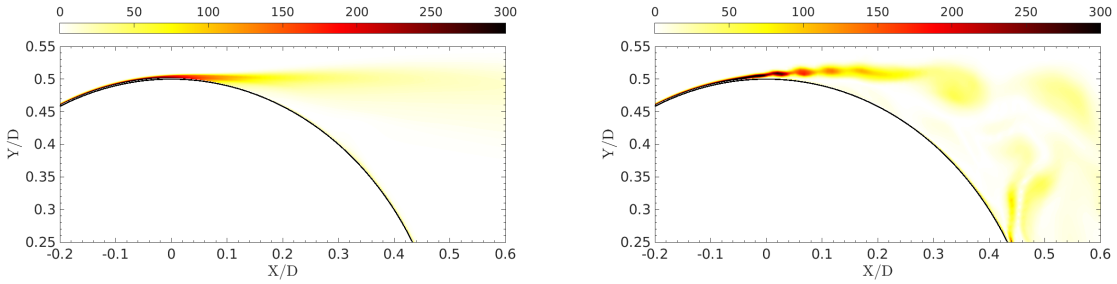

(a) $k-\omega$ SST DDES. **(b) LEBKE-SRH.**

Fig. 11 Instantaneous realisation of spanwise vorticity ω_k in free shear layer limited to $300s^{-1}$.

2. Scale Resolving Hybrid results

Simulations of a novel scale-resolving hybrid (SRH) model have also been conducted on the same mesh as for the RANS simulations and DDES. The SRH model based on both the $k-\omega$ SST model and Lag EB $k-\epsilon$ model is considered in this numerical study.

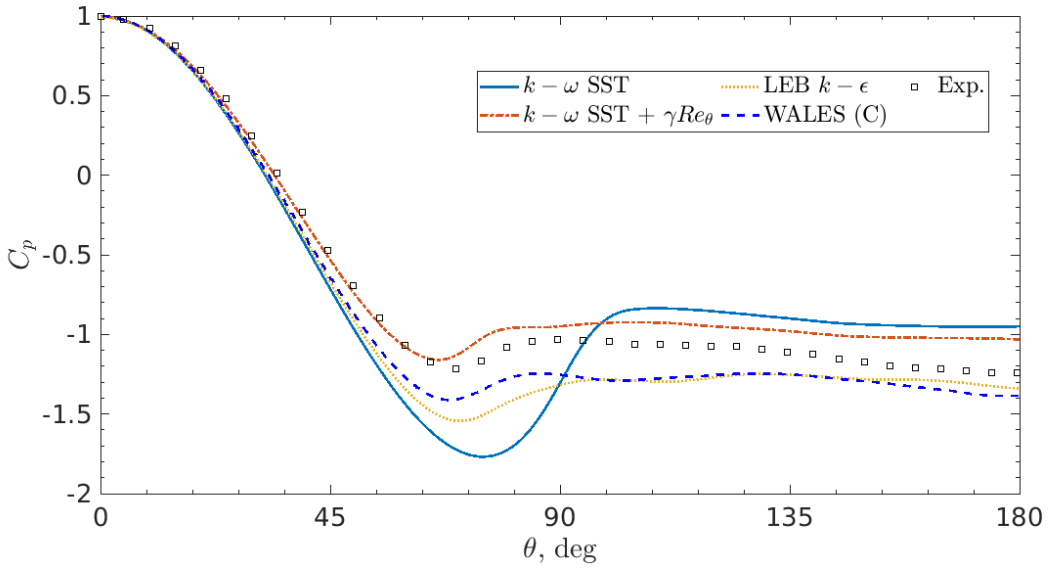

Fig. 12 Time-averaged pressure coefficient C_P distribution around cylinder for SRH closure models with WALES (C) and experimental reference data [29].

As seen in Fig. 13 and in Table 2, the $k-\omega$ SST SRH offers a slight improvement in comparison with the URANS base model for the time-averaged drag coefficient. However, the overall qualitative behaviour of the model is still more in

line with the $k-\omega$ URANS than the reference data. The continued discrepancy with the experimental values can again be attributed to the tendency of the URANS base model to prematurely predict transition to turbulence in the boundary layer. The application of the $\gamma Re\theta$ transition model serves to mitigate this effect and brings significant improvement in the results. The qualitative behaviour of the model matches the reference experimental and WALES LES data much more closely, visible in Fig. 13, and in the quantitative force values from Table 2, with the only apparent failure being an over-prediction of the back pressure of the cylinder leading to a raising of the C_p profile and an under-prediction of the time-averaged drag coefficient.

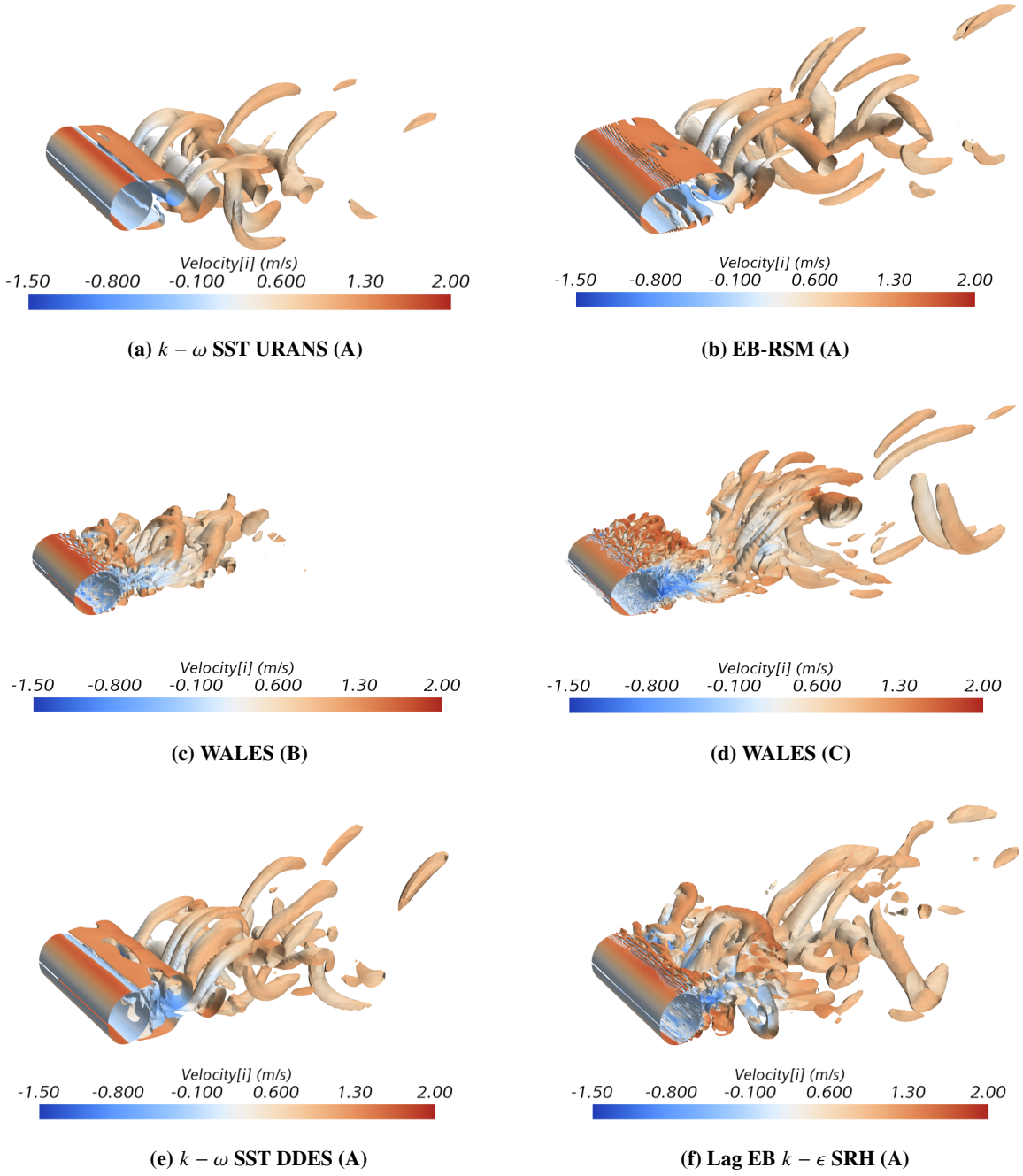

(a) $k-\omega$ **SST URANS (A)** **(b) EB-RSM (A)**

(c) WALES (B) **(d) WALES (C)**

(e) $k-\omega$ **SST DDES (A)** **(f) Lag EB** $k-\epsilon$ **SRH (A)**

Fig. 13 Iso-surfaces of instantaneous realisation of Q-criterion ($Q = 0.5$) coloured by streamwise velocity for major models with mesh indicated in brackets.

In marked contrast, the SRH model using the Lag EB $k-\epsilon$ as its basis RANS model shows a good performance. The shear layer breakdown observed in Fig. 13 for the Lag EB $k-\epsilon$ model is qualitatively similar to that observed in the high-resolution WALES LES case, notably on a far coarser mesh. The structures display a degree of stratification in the spanwise direction but this is attributable to the significant under-resolution in the spanwise direction. This appears to have no effect on the overall results indicating a significant robustness on the part of the model, which is confirmed by the observed C_p distribution in Fig. 12 and the predicted force values in Table 2, with the predicted time-averaged drag coefficient value within 5% of the WALES LES predicted value obtained on mesh C. Another result of note is the boundary layer profiles in Fig. 4. Here we see that the LEBKE-SRH gives similar results to the EB-RSM model in the near-wall region, which is expected given that both models behave as elliptically blended URANS models in that area. As the free-stream is approached the LEBKE-SRH boundary layer profiles are more aligned with the WALES (C) result than the URANS models. This again demonstrates that the SRH model behaves in the desired fashion.

Additionally, very low levels of sub-grid viscosity are seen in Table 3, especially in comparison to the URANS results. This is comparable to the magnitude of the ν_{sgs} in the WALE LES results both in the shear layer and wake regions with no evidence of any erroneous presence in the attached boundary layers. The qualitative distribution of the sub-grid viscosity in Fig. 9 for the SRH model is also similar to the WALES (C) result, with the maximal values dispersed throughout the far wake, unlike the DDES model which, like URANS, shows a concentrated zone in the re-circulation bubble. Overall, this indicates an excellent behaviour for the SRH based closure model which is free of any issues with premature transition and shows comparable ability to resolve unsteady structures, all on a mesh of approximately 5.6 times fewer cells than the WALE LES mesh.

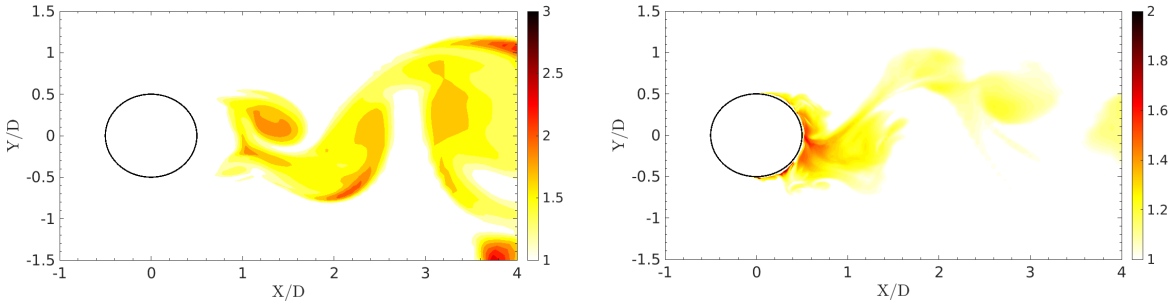

(a) DDES correction factor ϕ. **(b) SRH correction factor ψ.**

Fig. 14 Instantaneous realisation of correction functions for hybrid RANS/LES models.

The key difference apparent here between the DDES and SRH models is in the shielding formulation. As with DDES, the implementation of shielding plays an important role in the SRH model. The two models, however, have different implementations of the shield as highlighted by Figs 14a and 14b. These figures do not show the shielding directly but indicate the parameters relevant to each model which indicate LES-like behaviour. By comparing the two figures we see that a crucial difference between the DDES and SRH is that the SRH model switches to LES-like behaviour much nearer to the wall and in particular shortly after the detaching of the shear layer. This allows instability to develop early in the shear layer and the development of the breakdown mechanism of the shear layer is then simulated accurately. The SRH results in general are very strong with good agreement with experimental data across a range of quantities, even on coarse meshes. In particular the Lag EB $k-\epsilon$ SRH implementation is highly convenient as the underlying URANS formulation provides the improvement in the prediction of transition and non-linear effects. The $k-\omega$ SST SRH model requires the transition model for effective results which requires a degree of user specification and, further, the alteration of the underlying constitutive equation to account for non-linear effects. Overall, for robustness, convenience and low computational cost the Lag EB $k-\epsilon$ SRH model appears to be a strong choice for simulating highly-separated external flow.

V. Conclusion

The results presented in this study highlight that the chosen test case is highly sensitive to the numerical methods used to perform the simulations. Regarding the turbulence model, RANS methods - linear eddy and Reynolds Stress models - were unable to achieve a decent agreement with experimental reference data with the numerical schemes considered in the study. This failure carried through to runs utilising the DDES variant of the DES model. This is in large part due to the specific formulation of the DDES shielding function that prevented the formation of instabilities in the free shear layer. On the contrary, the WALE LES model proved successful on a sufficiently refined mesh, accurately predicting both time-averaged force and pressure coefficients and the behaviour of the shear layer breakdown. Whilst improving stability in a general sense, the introduction of upwinding of even a low amount into the BCD scheme degraded the results of LES simulations. Simulations with no introduced upwinding but bounded proved the most effective choice for an LES approach, showing no stability issues and improved accuracy. Finally, the results from the Scale Resolving Hybrid (SRH) model demonstrated robustness, with a good agreement with experiment reference data on the coarse mesh. The results were in line with the WALES LES method, but at only a fraction of the cost. The significant reduction in computational demand made possible by the SRH model makes it a strong choice for use in the simulation of highly separated flow, at least for the range of Reynolds number considered in the present study (around the drag crisis). Further investigations at various Reynolds numbers will look into the ability of the SRH model to capture accurately the drag crisis. As discussed in [3], the exact onset and conclusion points of the critical regime is highly sensitive to slight disturbances, such as free-stream turbulence or cylinder roughness, resulting in a significant scattering of numerical and experimental data for critical and super-critical drag coefficients. The ability of the most recent turbulence models (such as the SRH model) to accurately capture these regime transitions at a reasonable computational cost needs to be explored.

References

[1] Breuer, M., "A challenging test case for large eddy simulation: High Reynolds number circular cylinder flow," *International Journal of Heat and Fluid Flow*, Vol. 21, 2000, pp. 648–654. https://doi.org/10.1016/S0142-727X(00)00056-4.

[2] Moussaed, C., Salvetti, M. V., Wornom, S., Koobus, B., and Dervieux, A., "Simulation of the flow past a circular cylinder in the supercritical regime by blending RANS and variational-multiscale LES models," *Journal of Fluids and Structures*, Vol. 47, 2014, pp. 114–123.

[3] Rodríguez, I., Lehmkuhl, O., Chiva, J., Borrell, R., and Oliva, A., "On the flow past a circular cylinder from critical to super-critical Reynolds numbers: Wake topology and vortex shedding," *International Journal of Heat and Fluid Flow*, Vol. 55, 2015, pp. 91–103. https://doi.org/10.1016/j.ijheatfluidflow.2015.05.009.

[4] Palkin, E., Mullyadzhanov, R., Hadžiabdić, M., and Hanjalić, K., "Scrutinizing URANS in shedding flows: the case of cylinder in cross-flow in the subcritical regime," *Flow, Turbulence and Combustion*, Vol. 97, No. 4, 2016, pp. 1017–1046.

[5] Pereira, F. S., Eça, L., Vaz, G., and Girimaji, S. S., "Challenges in scale-resolving simulations of turbulent wake flows with coherent structures," *Journal of Computational Physics*, Vol. 363, 2018, pp. 98–115.

[6] Pereira, F. S., Eça, L., Vaz, G., and Girimaji, S. S., "On the simulation of the flow around a circular cylinder at R e = 140 , 000," *International Journal of Heat and Fluid Flow*, Vol. 76, 2019, pp. 40–56. https://doi.org/10.1016/j.ijheatfluidflow.2019.01.007, URL https://linkinghub.elsevier.com/retrieve/pii/S0142727X18306180.

[7] Smagorinsky, J., "General circulation experiments with the primitive equations: I. The basic experiment," *Monthly weather review*, Vol. 91, No. 3, 1963, pp. 99–164.

[8] Germano, M., Piomelli, U., Moin, P., and Cabot, W. H., "A dynamic subgrid-scale eddy viscosity model," *Physics of Fluids A: Fluid Dynamics*, Vol. 3, No. 7, 1991, pp. 1760–1765.

[9] Nicoud, F., and Ducros, F., "Subgrid-scale stress modelling based on the square of the velocity gradient tensor," *Flow, turbulence and Combustion*, Vol. 62, No. 3, 1999, pp. 183–200.

[10] Palkin, E., Mullyadzhanov, R., Hadžiabdić, M., and Hanjalić, K., "Scrutinizing URANS in Shedding Flows: The Case of Cylinder in Cross-Flow in the Subcritical Regime," *Flow, Turbulence and Combustion*, Vol. 97, No. 4, 2016. https://doi.org/10.1007/s10494-016-9772-z.

[11] Menter, F. R., Kuntz, M., and Langtry, R., "Ten years of industrial experience with the SST turbulence model," *Turbulence, heat and mass transfer*, Vol. 4, No. 1, 2003, pp. 625–632.

[12] Langtry, R. B., and Menter, F. R., "Correlation-based transition modeling for unstructured parallelized computational fluid dynamics codes," *AIAA journal*, Vol. 47, No. 12, 2009, pp. 2894–2906.

[13] Dol, H., Kok, J., and Oskam, B., "Turbulence modelling for leading-edge vortex flows," *40th AIAA Aerospace Sciences Meeting & Exhibit*, 2002, p. 843.

[14] Gritskevich, M. S., Garbaruk, A. V., Schütze, J., and Menter, F. R., "Development of DDES and IDDES formulations for the k-ω shear stress transport model," *Flow, turbulence and combustion*, Vol. 88, No. 3, 2012, pp. 431–449.

[15] Kok, J., Dol, H., Oskam, B., and van der Ven, H., "Extra-large eddy simulation of massively separated flows," *42nd AIAA Aerospace Sciences Meeting and Exhibit*, 2004, p. 264.

[16] Girimaji, S. S., "Partially-Averaged Navier-Stokes Model for Turbulence: A Reynolds-Averaged Navier-Stokes to Direct Numerical Simulation Bridging Method," *Journal of Applied Mechanics*, Vol. 73, No. 3, 2006, p. 413. https://doi.org/10.1115/1.2151207, URL http://AppliedMechanics.asmedigitalcollection.asme.org/article.aspx?articleid=1415576.

[17] Duffal, V., De Laage de Meux, B., and Manceau, R., "Development and validation of a hybrid RANS-LES approach based on temporal filtering," *ASME-JSME-KSME 2019 8th Joint Fluids Engineering Conference, AJKFluids 2019*, Vol. 2, 2019. https://doi.org/10.1115/AJKFluids2019-4937.

[18] Menter, F. R., "Two-equation eddy-viscosity turbulence models for engineering applications," *AIAA journal*, Vol. 32, No. 8, 1994, pp. 1598–1605.

[19] Menter, F. R., Langtry, R. B., Likki, S. R., Suzen, Y. B., Huang, P. G., and Völker, S., "A correlation-based transition model using local variables - Part I: Model formulation," *Journal of Turbomachinery*, 2006. https://doi.org/10.1115/1.2184352.

[20] Lardeau, S., and Billard, F., "Development of an elliptic-blending lag model for industrial applications," *54th AIAA Aerospace Sciences Meeting*, 2016, p. 1600.

[21] Manceau, R., and Hanjalić, K., "Elliptic blending model: A new near-wall Reynolds-stress turbulence closure," *Physics of Fluids*, Vol. 14, No. 2, 2002, pp. 744–754.

[22] Zdravkovich, M. M., *Flow around circular cylinders*, Oxford University Press, 1997.

[23] "Simcenter Star-CCM+," "https://www.plm.automation.siemens.com/global/en/products/simcenter/STAR-CCM.html", 2021. Documentation.

[24] Manceau, R., and Hanjalić, K., "Elliptic blending model: A new near-wall Reynolds-stress turbulence closure," *Physics of Fluids*, Vol. 14, No. 2, 2002. https://doi.org/10.1063/1.1432693.

[25] Travin, A., Shur, M., Strelets, M., and Spalart, P. R., "Physical and Numerical Upgrades in the Detached-Eddy Simulation of Complex Turbulent Flows," *Advances in LES of Complex Flows*, Springer, 2005. https://doi.org/10.1007/0-306-48383-1{_}16.

[26] Shur, M. L., Spalart, P. R., Strelets, M. K., and Travin, A. K., "A hybrid RANS-LES approach with delayed-DES and wall-modelled LES capabilities," *International Journal of Heat and Fluid Flow*, Vol. 29, No. 6, 2008, pp. 1638–1649. https://doi.org/10.1016/j.ijheatfluidflow.2008.07.001.

[27] Lilly, D. K., "A proposed modification of the Germano subgrid-scale closure method," *Citation: Physics of Fluids A: Fluid Dynamics*, Vol. 4, No. 3, 1992, p. 633. https://doi.org/10.1063/1.858280, URL https://doi.org/10.1063/1.858280.

[28] Parnaudeau, P., Carlier, J., Heitz, D., and Lamballais, E., "Experimental and numerical studies of the flow over a circular cylinder at Reynolds number 3900," *Physics of Fluids*, 2008. https://doi.org/10.1063/1.2957018.

[29] Cantwell, B., and Coles, D., "An experimental study of entrainment and transport in the turbulent near wake of a circular cylinder," *Journal of Fluid Mechanics*, Vol. 136, 1983, pp. 321–374. https://doi.org/10.1017/S0022112083002189.

[30] Wilcox, D. C., "Turbulence Modeling for CFD (Third Edition)," *DCW Industries*, , No. 1, 2006.

[31] Cheung, J. C., and Melbourne, W. H., "Turbulence effects on some aerodynamic parameters of a circular cylinder at supercritical numbers," *Journal of Wind Engineering and Industrial Aerodynamics*, Vol. 14, 1983, pp. 399–410. https://doi.org/10.1016/0167-6105(83)90041-7.

[32] Pont-Vílchez, A., Duben, A., Gorobets, A., Revell, A., Oliva, A., and Trias, F. X., "New Strategies for Mitigating the Gray Area in Delayed-Detached Eddy Simulation Models," *AIAA Journal*, 2021. https://doi.org/10.2514/1.j059666.